2.3 µm range InP-based type-II quantum well Fabry-Perot lasers heterogeneously integrated on a silicon photonic integrated circuit

Ruijun Wang,[1,2,*] **Stephan Sprengel,**[3] **Gerhard Boehm,**[3] **Muhammad Muneeb,**[1,2] **Roel Baets,**[1,2] **Markus-Christian Amann,**[3] **and Gunther Roelkens**[1,2]

[1]*Photonics Research Group, Ghent University-imec, Technologiepark-Zwijnaarde 15, 9052 Ghent, Belgium*
[2]*Center for Nano- and Biophotonics (NB-Photonics), Ghent University, Ghent, Belgium*
[3]*Walter Schottky Institut, Technische Universität München, Am Coulombwall 4, 85748 Garching, Germany*
[*]*Ruijun.Wang@intec.ugent.be*

Abstract: Heterogeneously integrated InP-based type-II quantum well Fabry-Perot lasers on a silicon waveguide circuit emitting in the 2.3 µm wavelength range are demonstrated. The devices consist of a "W"-shaped InGaAs/GaAsSb multi-quantum-well gain section, III-V/silicon spot size converters and two silicon Bragg grating reflectors to form the laser cavity. In continuous-wave (CW) operation, we obtain a threshold current density of 2.7 kA/cm^2 and output power of 1.3 mW at 5 °C for 2.35 µm lasers. The lasers emit over 3.7 mW of peak power with a threshold current density of 1.6 kA/cm^2 in pulsed regime at room temperature. This demonstration of heterogeneously integrated lasers indicates that the material system and heterogeneous integration method are promising to realize fully integrated III-V/silicon photonics spectroscopic sensors in the 2 µm wavelength range.

References and links

1. L. S. Rothman, I. E. Gordon, Y. Babikov, A. Barbe, D. Chris Benner, P. F. Bernath, M. Birk, L. Bizzocchi, V. Boudon, L. R. Brown, A. Campargue, K. Chance, E. A. Cohen, L. H. Coudert, V. M. Devi, B. J. Drouin, A. Fayt, J.-M. Flaud, R. R. Gamache, J. J. Harrison, J.-M. Hartmann, C. Hill, J. T. Hodges, D. Jacquemart, A. Jolly, J. Lamouroux, R. J. Le Roy, G. Li, D. A. Long, O. M. Lyulin, C. J. Mackie, S. T. Massie, S. Mikhailenko, H. S. P. Müller, O. V. Naumenko, A. V. Nikitin, J. Orphal, V. Perevalov, A. Perrin, E. R. Polovtseva, C. Richard, M. A. H. Smith, E. Starikova, K. Sung, S. Tashkun, J. Tennyson, G. C. Toon, V. G. Tyuterev, and G. Wagner, "The HITRAN2012 molecular spectroscopic database," J. Quant. Spectrosc. Radiat. Transf. **130**, 4–50 (2013).
2. A. Z. Subramanian, E. Ryckeboer, A. Dhakal, F. Peyskens, A. Malik, B. Kuyken, H. Zhao, S. Pathak, A. Ruocco, A. De Groote, P. Wuytens, D. Martens, F. Leo, W. Xie, U. D. Dave, M. Muneeb, P. Van Dorpe, J. Van Campenhout, W. Bogaerts, P. Bienstman, N. Le Thomas, D. Van Thourhout, Z. Hens, G. Roelkens, and R. Baets, "Silicon and silicon nitride photonic circuits for spectroscopic sensing on-a-chip," Photonics Res. **5**(3), 47–59 (2015).
3. G. Roelkens, U. Dave, A. Gassenq, N. Hattasan, B. Chen Hu, F. Kuyken, A. Leo, M. Malik, E. Muneeb, D. Ryckeboer, S. Sanchez, R. Uvin, Z. Wang, R. Hens, Y. Baets, F. Shimura, B. Gencarelli, R. Vincent, J. Loo, L. Van Campenhout, J.-B. Cerutti, E. Rodriguez, M. Tournie, Xia Chen, M. Nedeljkovic, G. Mashanovich, Li Shen, N. Healy, A. C. Peacock, Xiaoping Liu, R. Osgood, and W. M. J. Green, "Silicon-based photonic integration beyond the telecommunication wavelength range," IEEE J. Sel. Top. Quantum Electron. **20**(4), 394–404 (2014).
4. G. Z. Mashanovich, F. Y. Gardes, D. J. Thomson, Y. Hu, M. Ke Li, J. Nedeljkovic, A. Z. Soler Penades, C. J. Khokhar, S. Mitchell, R. Stankovic, S. A. Topley, B. Reynolds, Y. Wang, V. M. N. Troia, C. G. Passaro, T. Littlejohns, D. Bucio, P. R. Wilson, and G. T. Reed, "Silicon photonic waveguides and devices for near- and mid-IR applications," IEEE J. Sel. Top. Quantum Electron. **21**(4), 8200112 (2015).
5. Z. Zhou, B. Yin, and J. Michel, "On-chip light sources for silicon photonics," Light Sci. Appl. **4**(11), e358 (2015).
6. Z. Wang, B. Tian, M. Pantouvaki, W. Guo, P. Absil, J. Van Campenhout, C. Merckling, and D. Van Thourhout, "Room-temperature InP distributed feedback laser array directly grown on silicon," Nat. Photonics **9**(12), 837–842 (2015).

7. L. Cerutti, J. B. Rodriguez, and E. Tournie, "GaSb-based laser, monolithically grown on silicon substrate, emitting at 1.55um at room temperature," IEEE Photonics Technol. Lett. **22**(8), 553–555 (2010).
8. G. Roelkens, A. Abassi, P. Cardile, U. Dave, A. de Groote, Y. de Koninck, S. Dhoore, X. Fu, A. Gassenq, N. Hattasan, Q. Huang, S. Kumari, S. Keyvaninia, B. Kuyken, L. Li, P. Mechet, M. Muneeb, D. Sanchez, H. Shao, T. Spuesens, A. Subramanian, S. Uvin, M. Tassaert, K. van Gasse, J. Verbist, R. Wang, Z. Wang, J. Zhang, J. van Campenhout, J. Bauwelinck, G. Morthier, R. Baets, D. van Thourhout, and X. Yin, "III-V-on-Silicon photonic devices for optical communication and sensing," Photonics **2**(3), 969–1004 (2015).
9. D. Liang, G. Roelkens, R. Baets, and J. Bowers, "Hybrid integrated platforms for silicon photonics," Materials (Basel) **3**(3), 1782–1802 (2010).
10. K. Ohashi, K. Nishi, T. Shimizu, M. Nakada, J. Fujikata, J. Ushida, S. Torii, K. Nose, M. Mizuno, H. Yukawa, M. Kinoshita, N. Suzuki, A. Gomyo, T. Ishi, D. Okamoto, K. Furue, T. Ueno, T. Tsuchizawa, T. Watanabe, K. Yamada, S. I. Itabashi, and J. Akedo, "On-Chip Optical Interconnect," Proc. IEEE **97**(7), 1186–1198 (2009).
11. A. Spott, J. Peters, M. L. Davenport, E. J. Stanton, C. D. Merritt, W. W. Bewley, I. Vurgaftman, C. S. Kim, J. R. Meyer, J. Kirch, L. J. Mawst, D. Botez, and J. E. Bowers, "Quantum cascade laser on silicon," Optica **3**(5), 545–551 (2016).
12. A. Spott, J. Peters, M. L. Davenport, E. J. Stanton, C. Zhang, C. D. Merritt, W. W. Bewley, I. Vurgaftman, C. S. Kim, J. R. Meyer, J. Kirch, L. J. Mawst, D. Botez, and J. E. Bowers, "Heterogeneously Integrated Distributed Feedback Quantum Cascade Lasers on Silicon," Photonics **3**(2), 35 (2016).
13. A. Spott, M. Davenport, J. Peters, J. Bovington, M. J. R. Heck, E. J. Stanton, I. Vurgaftman, J. Meyer, and J. Bowers, "Heterogeneously integrated 2.0 μm CW hybrid silicon lasers at room temperature," Opt. Lett. **40**(7), 1480–1483 (2015).
14. G. Boehm, M. Grau, O. Dier, K. Windhorn, E. Roenneberg, J. Rosskopf, R. Shau, R. Meyer, M. Ortsiefer, and M. C. Amann, "Growth of InAs- containing quantum wells for InP-based VCSELs emitting at 2.3 μm," J. Cryst. Growth **301–302**, 941–944 (2007).
15. S. Sprengel, G. Veerabathran, A. Andrejew, A. Köninger, G. Boehm, C. Grasse, and M. C. Amann, "InP-based type-II heterostructure lasers for wavelengths up to 2.7 μm," in *SPIE Photonics West, Novel In-Plane Semiconductor Lasers XIV* (SPIE, 2015), paper 9382–29.
16. S. Sprengel, A. Andrejew, K. Vizbaras, T. Gruendl, K. Geiger, G. Boehm, C. Grasse, and M.-C. Amann, "Type-II InP-based lasers emitting at 2.55 μm," Appl. Phys. Lett. **100**(4), 041109 (2012).
17. C. Grasse, P. Wiecha, T. Gruendl, S. Sprengel, R. Meyer, and M.-C. Amann, "InP-based 2.8–3.5 μm resonant-cavity light emitting diodes based on type-II transitions in GaInAs/GaAsSb heterostructures," Appl. Phys. Lett. **101**(22), 221107 (2012).
18. S. Sprengel, C. Grasse, P. Wiecha, A. Andrejew, T. Gruendl, G. Boehm, R. Meyer, and M.-C. Amann, "InP-Based Type-II Quantum-Well Lasers and LEDs," IEEE J. Sel. Top. Quantum Electron. **19**(4), 1900909 (2013).
19. R. Wang, S. Sprengel, M. Muneeb, G. Boehm, R. Baets, M. C. Amann, and G. Roelkens, "2 μm wavelength range InP-based type-II quantum well photodiodes heterogeneously integrated on silicon photonic integrated circuits," Opt. Express **23**(20), 26834–26841 (2015).
20. R. Wang, M. Muneeb, S. Sprengel, G. Boehm, A. Malik, R. Baets, M.-C. Amann, and G. Roelkens, "III-V-on-silicon 2-μm-wavelength-range wavelength demultiplexers with heterogeneously integrated InP-based type-II photodetectors," Opt. Express **24**(8), 8480–8490 (2016).
21. S. Keyvaninia, M. Muneeb, S. Stanković, P. J. Van Veldhoven, D. Van Thourhout, and G. Roelkens, "Ultra-thin DVS-BCB adhesive bonding of III–V wafers, dies and multiple dies to a patterned silicon-on-insulator substrate," Opt. Mater. Express **3**(1), 35–46 (2013).

1. Introduction

The spectral range of 2-3 μm is of interest for security, environmental and process control applications since many important gases have strong absorption lines in this wavelength range [1]. For example, the wavelength range around 2.3 μm offers the first water absorption free spectral window for CO detection. Integrated photonics promises to enable the realization of miniaturized real-time sensors to detect of a variety of such substances on a compact photonic chip [2]. As one of the most prominent integrated photonics platforms, silicon photonics has been attracting a lot of attention over the past decade as it takes advantage of mature CMOS processes, allowing the fabrication of large scale photonic integrated circuits (PICs) at low cost. A number of passive silicon photonics components operating in the 2 μm wavelength range have been demonstrated in recent years [3,4]. However, a fully integrated silicon photonics sensor system still is to be demonstrated due to the limited development of active devices integrated on silicon in this wavelength range. In recent years a few approaches have been developed to integrate active opto-electronic devices on silicon, especially at optical communication wavelengths, e.g., the direct epitaxial growth of III-V or Ge material, the bonding of III-V material onto silicon and the flip-chip integration of prefabricated devices [5–10]. Among these approaches, the heterogeneous integration of III-V material on silicon

by adhesive bonding or molecular bonding has proven to be an appealing way to integrate lasers on silicon photonic ICs [8,9]. Quantum cascade lasers operating in pulsed regime heterogeneously integrated on a silicon-on-nitride-on-insulator waveguide circuit were demonstrated operating between 4.6 and 4.9 µm wavelength [11,12]. Heterogeneously integrated III-V/silicon lasers using strained InGaAs type-I heterostructures, operating at 2 µm wavelength and emitting up to 4.2 mW of single facet CW power at room temperature were also demonstrated [13]. However, the emission wavelength of highly strained quantum well structures on InP is limited to around 2.3 µm [14]. For the wavelength range above 2.3 µm, GaSb-based type-I heterostructures can be used to realize lasers with high performance. In previous work, we demonstrated a GaSb on silicon-on-insulator (SOI) cleaved 2.4 µm wavelength Fabry-Perot laser operating in pulsed regime at 10 °C [3]. The heterogeneous integration processes of InP-based materials and devices is, however, better-established compared with GaSb, allowing for high-yield processes and good device performance. In recent years, electrically pumped lasers using type-II heterostructures on an InP substrate were demonstrated up to a wavelength of 2.7 µm and with a threshold current density of 3.2 kA/cm^2 at 0 °C at a continuous wave (CW) lasing wavelength of 2.31 µm [15,16]. Besides, resonant-cavity light-emitting diodes operating up to 3.3 µm wavelength and photoluminescence up to 3.9 µm wavelength were reported based on this material system [17,18]. All of these results appear promising for the realization of III-V/silicon photonic ICs operating in the 2 µm or 3 µm wavelength range by bonding InP-based type-II heterostructures to a silicon waveguide circuit. Recently, we demonstrated an InP-based type-II quantum well photodetector array with responsivity up to 1.6 A/W at 2.35 µm wavelength and a dark current of 10 nA at −0.5 V bias, heterogeneously integrated on low insertion loss (−2.5 dB) and low-crosstalk (−30 dB) arrayed waveguide grating (AWG) spectrometers [19,20]. Here we present the heterogeneous integration of InP-based type-II quantum well Fabry-Perot lasers on a silicon photonic IC using benzo-cyclo-butene (DVS-BCB) adhesive bonding technology. The light is efficiently coupled from the III-V-on-silicon gain section to the silicon waveguide using a III-V/silicon spot size converter. The heterogeneously integrated type-II lasers emit in the 2.3 µm wavelength range. At 2.35 µm wavelength, an output power of 1.3 mW and threshold current density of 2.7 kA/cm^2 is obtained in a CW regime at 5 °C. Under pulsed operation, the lasers output over 3.7 mW peak power with a threshold current density of 1.6 kA/cm^2 at room temperature. This demonstration of heterogeneously integrated lasers indicates that the material system and heterogeneous integration method are promising to realize fully integrated III-V/silicon photonics spectroscopic sensors in the 2 µm wavelength range.

2. Design and Fabrication

The heterogeneously integrated InP-based type-II quantum well laser is schematically shown in Fig. 1(a) and 1(b). The III-V epitaxial structure is adhesively bonded to the SOI waveguide circuit using a 100 nm thick DVS-BCB layer as bonding agent. The device consists of a III-V gain section, III-V/silicon spot size converters and two distributed Bragg reflectors (DBR) implemented in an SOI waveguide. The laser cavity feedback is realized using a high reflectivity silicon DBR (DBR1, 20 periods, 435 nm period, duty cycle 50%, 180 nm etch depth) and a lower reflectivity silicon DBR (DBR2, 4 periods, 435 nm period, duty cycle 50%, 180 nm etch depth) used as output port. Simulation results indicate the DBR1 and DBR2 can provide ~90% and 32% reflectivity at 2.35 µm wavelength, respectively, as shown in Fig. 1(c). Due to the high refractive index contrast the bandwidth of the reflector is very large. In the center of the device the light is confined in the III-V waveguide as shown in Fig. 1(d), which provides maximum gain. Light is coupled from the III-V waveguide to the silicon waveguide by using a III-V/silicon spot size converter. At the III-V taper tip position, the light is completely coupled into the silicon waveguide as shown in Fig. 1(e).
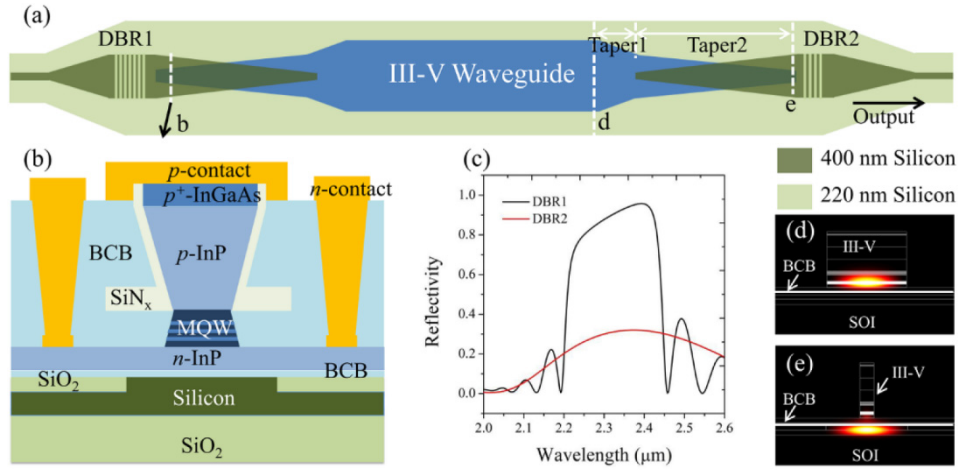
Fig. 1. (a) Schematic drawing of the top view of the InP-based type-II quantum well laser heterogeneously integrated on a SOI waveguide circuit, showing the III-V mesa and SOI waveguide structure. The electrical contacts were omitted for clarity; (b) detailed cross-section of the III-V/silicon waveguide; (c) simulated reflectivity of DBR1 and DBR2; (d) and (e) TE-polarized mode intensity distribution in different parts of the laser cavity, the position of which is marked in (a).

The III-V epitaxial structure is grown on an n-doped InP substrate with a molecular beam epitaxy (MBE) system. Figure 2(a) shows the band structure of the designed "W"-shaped layer structure. The epitaxial layer stack consists of a 200 nm thick n-InP contact layer, an active region sandwiched between a 130 nm thick GaAsSb and a 250 nm thick AlGaAsSb separate confinement heterostrctures layer, a 1.5 µm thick p-InP cladding layer and a 100 nm thick p^+-InGaAs contact layer. The active region consists of six periods of a "W"-shaped quantum well structure, each separated by 9 nm tensile strained $GaAs_{0.58}Sb_{0.42}$ layers. The quantum well structure consists of a 2.9 nm thick $GaAs_{0.33}Sb_{0.67}$ hole-confining layer surrounding by two 2.6 nm thick $In_{0.68}Ga_{0.32}As$ electron-confining layers. A 10 nm AlGaInAs layer and a 20 nm AlAsSb layer is used as hole blocking layer on the n-side and electron blocking layer on the p-side, respectively, to avoid electron and hole leakage from the active region. The same epitaxial layer stack has been used to realize heterogeneously integrated InP-based type-II quantum well photodetectors. More specific information about the "W"-shaped active region design can be found in [16,18].
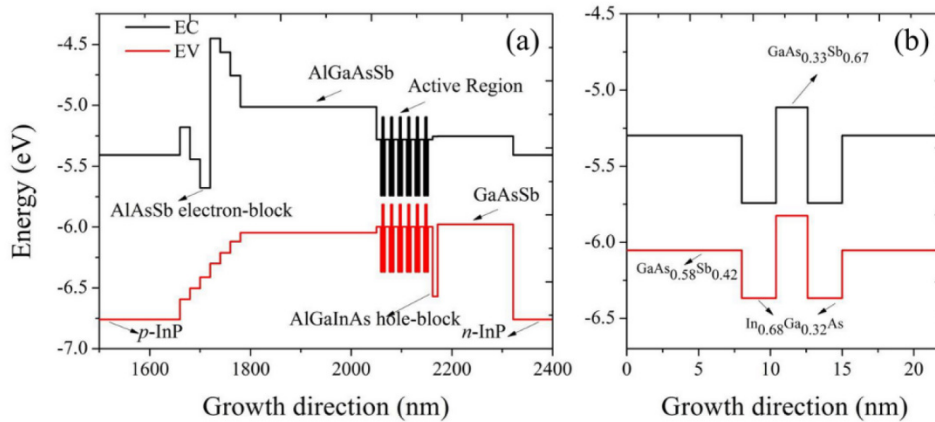

Fig. 2. (a) Biased band structure of the InP-based type-II laser on silicon; (b) magnification of one "W"-shaped period of the active region.

The mode intensity profiles and optical coupling efficiency are calculated using commercial software (FIMMWAVE) to optimize the device design. The rib silicon waveguide is 400 nm high with an etch depth of 180 nm. A 5 µm wide III-V mesa is chosen to obtain low waveguide loss and high optical confinement in the active region of the gain section. The calculated confinement factor of the TE polarized fundamental mode (at 2.35 µm wavelength) in the six quantum wells is 10.2%. An efficient optical coupling between the III-V waveguide and silicon waveguide is realized using III-V/silicon spot size converters by tapering both waveguides. The III-V/silicon spot size converter has two tapered sections as shown in Fig. 1(a). In the first taper section, the III-V waveguide is linearly tapered from 5 µm to 1.2 µm over a length of 50 µm. The second section is an adiabatic inverted taper coupler, where the III-V waveguide is slowly tapered to a very narrow tip while the silicon waveguide underneath is tapered from 200 nm to 3 µm. Figure 3(a) shows the coupling efficiency of the III-V/silicon spot size converter as a function of the III-V taper tip width. We can find that high coupling efficiency can be achieved when a 0.5 µm wide taper tip is used. Although 90 µm long tapers with 0.5 µm wide tip provide a coupling efficiency higher than 90% as shown in Fig. 3(b), 180 µm long tapers are used in the experiment to get a more robust coupling. The fundamental mode evolution in a longitudinal cross section of the 180 µm long III-V-on-silicon adiabatic taper with a 0.5 µm wide taper tip is shown in the inset picture of Fig. 3(a). The III-V/silicon spot size converters are electrical pumped during device operation to avoid optical loss as the III-V taper contains the same active region as in the gain section.
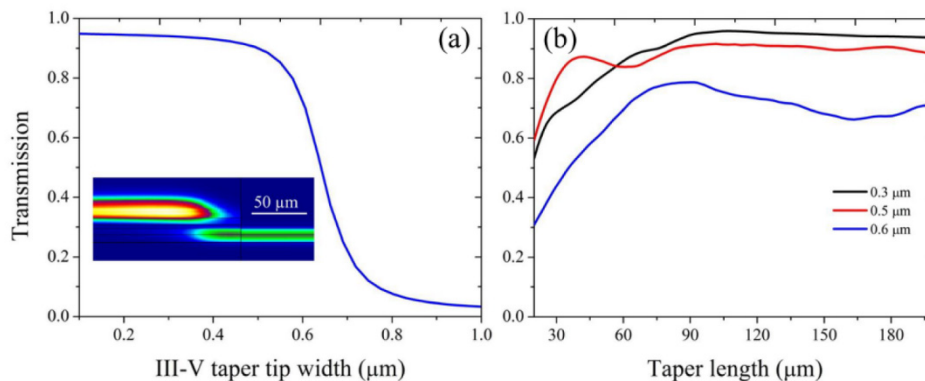

Fig. 3. (a) Simulated coupling efficiency of a 180 µm long adiabatic taper as a function of the taper tip width. The inset picture shows the fundamental mode intensity evolution in the 180 µm long adiabatic taper with 0.5 µm wide III-V taper tip; (b) coupling efficiency of the adiabatic tapers with different tip widths as a function of the taper length.

The general fabrication flow of the heterogeneously integrated InP-based type-II lasers on silicon is the same as the photodetector process flow described in [20]. The passive SOI waveguide circuit is processed in imec's CMOS pilot line on 200 mm SOI wafers. Silicon is etched 180 nm deep in the 400 nm thick silicon device layer (2 µm buried oxide layer thickness) for rib waveguide and grating fabrication. The silicon waveguide circuits are planarized by SiO_2 deposition followed by chemical mechanical polishing (CMP) down to the silicon device layer. The InP-based epitaxial stack is adhesively bonded to the SOI waveguide circuit using a 100 nm thick DVS-BCB layer [21]. After bonding, the InP substrate is removed using HCl wet etching. Then a 200 nm SiN_x layer is deposited on the sample as hard mask, which is patterned using 320 nm UV contact lithography. From the simulation, a narrow III-V taper tip is required to realize efficient coupling between the III-V waveguide and silicon waveguide. The key technological step to realize a III-V taper tip narrower than 500 nm using 320 nm UV contact lithography is to use an anisotropic HCl wet etching of the

p-InP layer, which creates an inverted trapezoidal mesa when the III-V waveguide is oriented along the [01-1] direction. This reduces the lithographic pattern size requirements. A 1 μm taper tip is defined in the SiN hard mask. After the hard mask patterning, the 100 nm p^+-InGaAs layer is etched by inductively-coupled plasma (ICP) and the 1.5 μm p-InP cladding layer is etched by a 1:1 HCl:H_2O solution. Then a SiN_x hard mask is deposited and patterned on the sample to cover the p-InP cladding layer to protect the III-V waveguide in the following quantum well wet etching. Afterwards, the GaAsSb cladding layer and active region are etched using a 1:1:20:70 H_3PO_4: H_2O_2: Citric Acid: H_2O solution. Then Ni/Ge/Au is deposited on the n-InP layer as n-contact, 5 μm away from the III-V mesa. After metal lift-off, devices are isolated by using 1:1 HCl:H_2O to etch the n-InP layer. Then DVS-BCB is spin-coated on the sample and cured for device passivation. Subsequent dry etching of BCB is carried out to open windows for n-contact and p-contact. Finally, Ti/Au is deposited as n-contact and p-contact probe pads. Figures 4(a) and 4(b) show the top view microscope image and scanning electron microscope (SEM) cross-section image of the heterogeneously integrated lasers on silicon waveguides, respectively. A common p-contact pad is used serving as a heat-spreader for the integrated lasers.
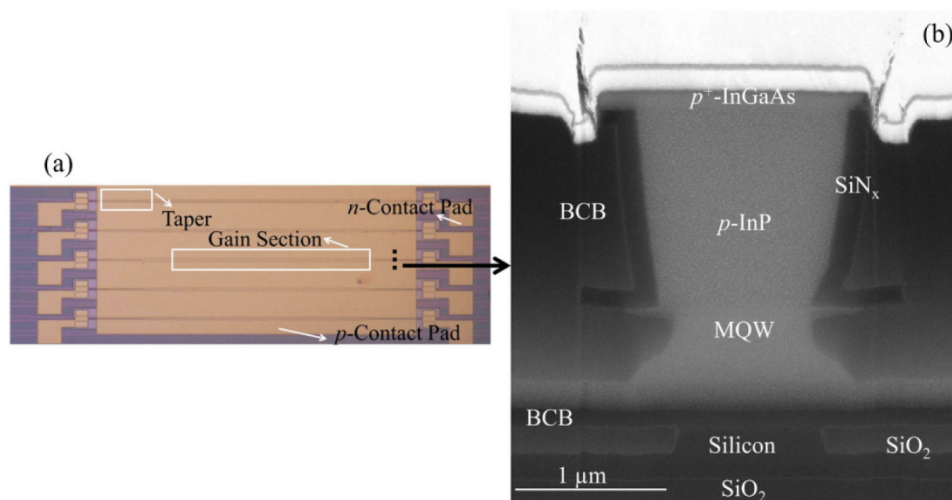

Fig. 4. (a) Microscope image of the heterogeneously integrated lasers; (b) SEM image of the cross-section of the device.

3. Measurement results

The fabricated heterogeneously integrated laser has a 1000 μm long gain section with an III-V waveguide width of 5 μm. The devices are characterized using DC and pulsed current sources. The light in the silicon waveguide is coupled out from a grating coupler and collected by a standard single mode fiber (SMF-28), which is connected to an optical spectrum analyzer (OSA, Yokogawa AQ6375). The laser power coupled into the silicon waveguide is calibrated by measuring the coupling efficiency of reference grating coupler structures. At 2.35 μm wavelength, the coupling efficiency is around −10 dB, and the 3 dB bandwidth is 150 nm. More detailed information about the grating coupler can be found in [19]. The samples are mounted on a temperature controller which allows the devices operating temperature to be varied from 0 °C to 80 °C. Figure 5 shows the L-I-V curve of the heterogeneously integrated laser with a DBR period of 435 nm under CW operation at 5 °C. A maximum optical output power of 1.3 mW coupled into the silicon waveguide is obtained. The laser has a threshold current of 135 mA, corresponding to a threshold current density of 2.7 kA/cm². The series resistance of the laser is 8.5 Ω. It can be reduced by optimizing the

metallization processes and reducing the gap between the III-V waveguide and n-InP (currently 5 μm). The slope efficiency near threshold current is 0.035 W/A at 5 °C.
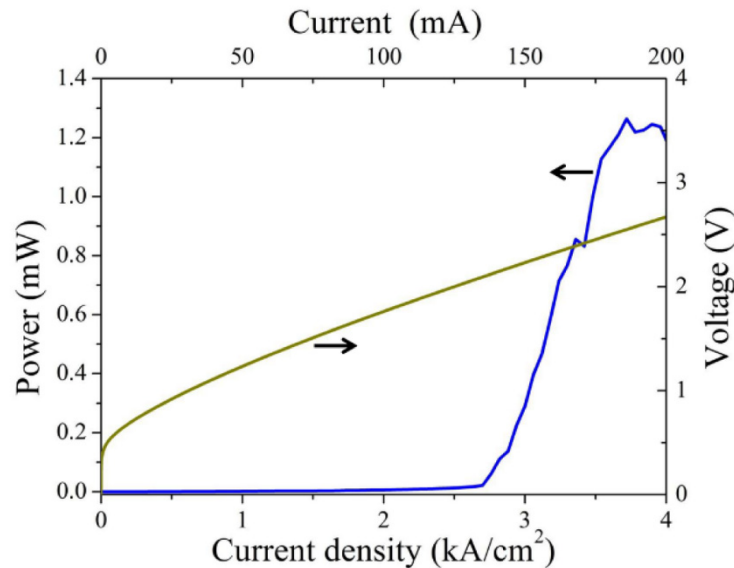

Fig. 5. I-V curve of the laser and CW output power as a function of drive current at 5 °C.

Figure 6(a) shows a typical amplified spontaneous emission (ASE) spectrum from a heterogeneously integrated semiconductor optical amplifier (SOA) integrated on the same chip, with the same dimensions as the gain section of the laser structure. A broadband emission with peak around 2.35 μm is obtained by collecting the light coupled out through the grating coupler. By implementing a cavity around the SOA using a high reflectivity DBR mirror (N_{per} = 20) and a partially reflecting DBR (N_{per} = 4), laser operation is obtained. Figure 6 (b) shows the emission spectra of two heterogeneously integrated lasers with different DBR period (420 nm and 435 nm), driven at an injection current of 160 mA at 5 °C in CW operation. The spectra are measured with a Yokogawa AQ6375 OSA with a resolution bandwidth of 0.1 nm. The longitudinal modes of the Fabry-Perot laser cavity can clearly be observed. As shown in Fig. 6(b), the lasing wavelength can be tuned by adjusting the grating period. The dominant lasing wavelength shifts from 2332.5 nm to 2351.3 nm when the DBR period increases from 420 nm to 435 nm. A close up of the lasing Fabry-Perot modes is shown in Fig. 6(c). The free spectral range of the longitudinal modes is 0.52 nm, which correspond to an average group index of 3.8 for an overall 1400 μm long Fabry-Perot cavity (with DBRs located 20 μm away from the III-V taper tip). A modulation of the intensity of the longitudinal modes can be observed, which is attributed to a parasitic reflection of the grating coupler structure used to couple light to single mode fiber. The side mode suppression ratio (SMSR) is around 17 dB for the Fabry-Perot lasers. Single mode lasing with higher SMSR can be achieved by replacing the broadband DBR with a narrow band reflector, or integrating an additional wavelength selective element in the cavity, such as a high quality factor microring resonator.
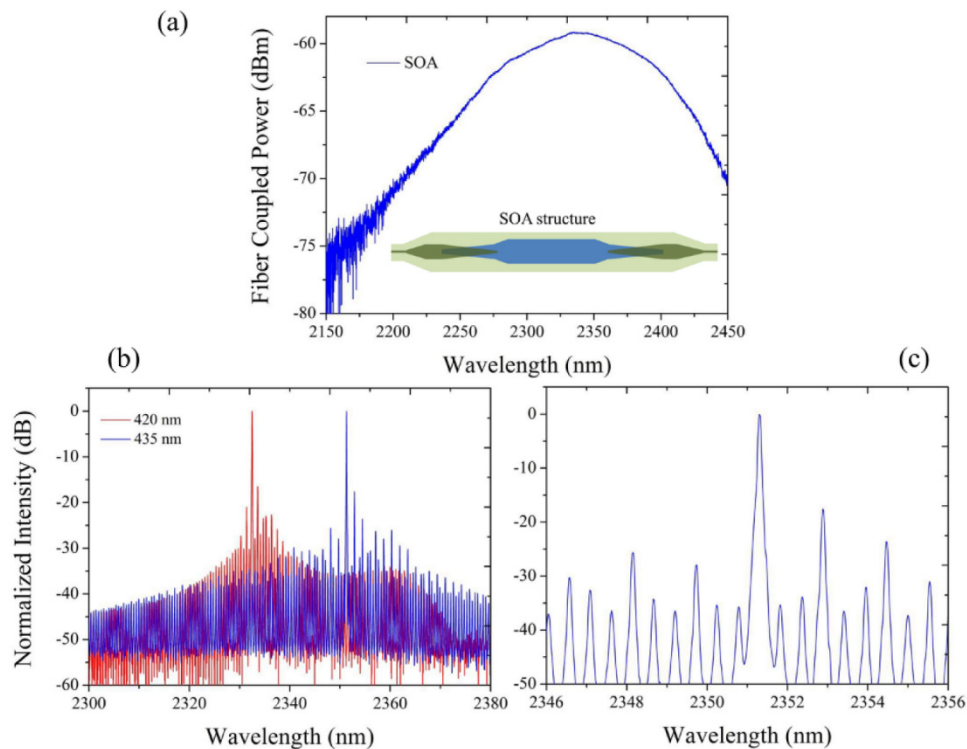
Fig. 6. (a) ASE spectrum from a heterogeneously integrated SOA (driven at 150 mA) on a silicon waveguide circuit (1 nm resolution). The SOA has the same structure and dimensions as the laser except no DBR is implemented, as shown in the inset; (b) two typical emission spectra from the heterogeneously integrated Fabry-Perot lasers with different DBR period (420 nm and 435 nm), characterized under CW operation at 5 °C and 160 mA injected current; (c) zoom of the emission spectrum from the Fabry-Perot laser with DBR period of 435 nm.

Under CW operation, the maximum operating temperature of the InP-based type-II lasers integrated on SOI is around 9 °C. This is attributed to the relatively high thermal impedance of the laser caused by the presence of the BCB bonding layer and buried oxide layer with low thermal conductivity, and to the relatively high electrical series resistance of the device, as discussed above. The lasing threshold and maximum operating temperature could be further improved by reducing the thermal resistance of the device. A 100 nm thick BCB layer is used in the device shown here, which can be reduced to 30 nm to 50 nm, which is the typical range used in heterogeneously integrated 1550 nm wavelength lasers with high performance. Reducing the buried oxide thickness or connecting the top heat spreader to the silicon substrate also can be used to reduce the thermal resistance. Besides, the carrier injection efficiency of the InP-based type-II epitaxial structure should be further enhanced to improve the maximum operating temperature [18].

Figure 7 shows the laser output power coupled to the silicon waveguide as a function of the injected pulsed current (pulse duration 0.5 μs, period of 50 μs) at a stage temperature ranging from 15 °C to 40 °C. As can be seen from the figure, the laser has a threshold current of 72 mA and a maximum (peak) output power of 4.7 mW at 15 °C. The inset in Fig. 7 plots the corresponding dependence of the threshold current density on temperature. The characteristic temperature T_0 is fitted to be 33K, which is in the typical range of 20K-50K for the recently demonstrated InP-based type-II lasers [16].
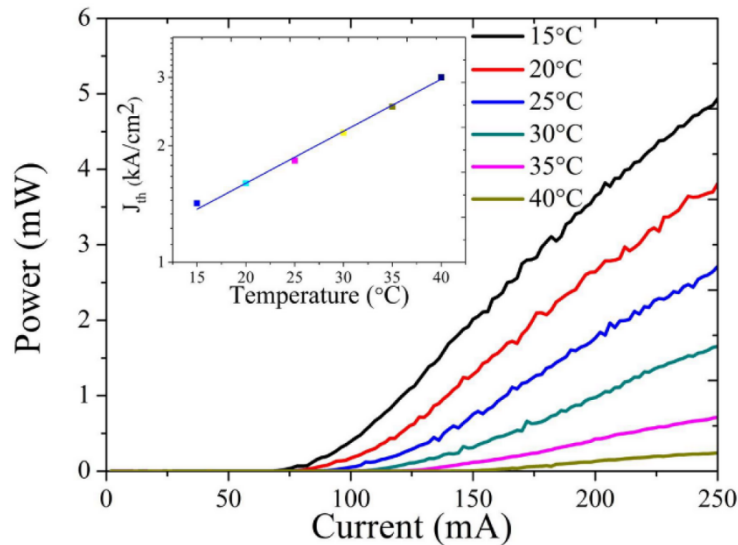
Fig. 7. Peak laser output power as a function of pulsed driving current at temperatures from 15 °C to 40 °C, for a pulse length of 0.5 μs and a repetition rate of 20 kHz. The inset picture shows the dependence of the pulsed threshold current density on temperature.

4. Conclusion

In this paper, we demonstrate for the first time the heterogeneous integration of InP-based type-II lasers on a silicon waveguide circuit for the 2.3 μm wavelength range. The Fabry-Perot laser cavity consists of a type-II multi-quantum-well gain region sandwiched between two SOI waveguide DBRs. A high efficiency III-V/silicon spot size converter is designed to realize light coupling between the III-V waveguide and silicon waveguide. In CW operation, the laser has a threshold current density of 2.7 kA/cm^2 and maximum light output power of 1.3 mW at 5 °C, at a wavelength of 2.35 μm. For pulsed operation, a threshold current density of 1.6 kA/cm^2 and output power of 3.7 mW is obtained at room temperature. Further improvements on epitaxial layer design, BCB thickness and heat sinking are expected to improve device performance further. With previously demonstrated photodetector arrays and AWG spectrometers on silicon, this demonstration of heterogeneously integrated lasers establishes a path to integrated on-chip spectroscopic sensors in the 2 μm wavelength range.

Acknowledgments